IEEE Access
Multidisciplinary ⋮ Rapid Review ⋮ Open Access Journal

Received 17 March 2023, accepted 9 April 2023, date of publication 19 April 2023, date of current version 9 May 2023.

Digital Object Identifier 10.1109/ACCESS.2023.3268227

RESEARCH ARTICLE

Modeling Phase Changing Property of VO_2 for Reconfigurable Microwave Frequency Selection Applications via Time-Resolved Microwave Conductivity

QASSIM ABDULLAHI[1], (Student Member, IEEE), MOHAMMAD VASEEM[2], (Member, IEEE), ATIF SHAMIM[2], (Senior Member, IEEE), GEORGE GOUSSETIS[1], (Senior Member, IEEE), AND DIMITRIS E. ANAGNOSTOU[1], (Senior Member, IEEE)

[1]Institute of Signals, Sensors and Systems, Heriot-Watt University, EH14 4AS Edinburgh, U.K.
[2]Department of Electrical and Computer Engineering, King Abdullah University of Science and Technology, Thuwal 23955, Saudi Arabia

Corresponding author: Dimitris E. Anagnostou (d.anagnostou@hw.ac.uk)

This work was supported in part by the Defence and Security Accelerator project #ACC6003961, in part by the U.K. Research and Innovation (UKRI) Talent and Research Stabilization Fund under Grant UKRI IAA2022 VisionRF, and in part by the UKRI Innovation-to-Commercialization of University Research (ICURe) under Award NXW-EX-MAR23-01-Heriot-Watt.

ABSTRACT Vanadium dioxide (VO_2) is characterized using the time-resolved microwave conductivity (TRMC) method for applications requiring reconfigurable microwave frequency selection. We demonstrate that TRMC is a flexible method for determining the microwave conductivity of thin film compounds of varied thicknesses that are both phase-changing and non-phase changing in nature. The method makes use of Ka-band microwave resonant waveguides to examine how thermally excited samples' microwave conductivity changes in response to microwave-transmitted power through the system's sensitivity factor. The sensitivity factor is illustrated by a study of incident waves (electromagnetic fields) on medium and waveguide perturbation analysis in VO_2 thin films. The TRMC measurements show a low regime in the microwave conductivity below the transition temperature (T_c) of VO_2 where T_c occurs near 65°C; this is associated with the dielectric characteristics of the charge carriers and points to the presence of shallow trap electron states. Longer electron hops enhance charge mobility and, consequently, the barrier energy above T_c, where these states are thermally discharged, resulting in a high thermally triggered microwave conductivity regime. The activation energy may come from a variety of complex contributions, like polaronic self-localizations, as well as a dynamic disorder brought on by the thermal oscillations of VO_2 molecules. The calculated conductance values are simulated in CST Studio as plane wave incidence on medium to ascertain the fields' microwave transmission behavior and contrast it with the experimental results to validate the model. Additionally, using the derived conductivities, the characteristics of well-known materials like copper (Cu) were confirmed.

INDEX TERMS Frequency selective surfaces, reconfigurable components, time resolved microwave conductivity, vanadium dioxide.

I. INTRODUCTION

Phase-changing compounds such as vanadium dioxide (VO_2) can reversibly change their electrical and optical properties between insulating (M_1) to conducting metallic states (R) triggered by external stimuli [1]. The most used stimulus to promote VO_2 insulator-to-metal transition (IMT) is temperature. The entropy-driven transition of metallic state occurs at elevated temperatures, aggravating the physical and chemical properties of VO_2 such as a change in their optical, electrical, thermal, and magnetic properties [2]. The phase transition occurs when the applied temperature within dense arrays of

The associate editor coordinating the review of this manuscript and approving it for publication was Wanchen Yang.

VO_2 molecules overcomes a certain threshold of about 341°K (68°C) known as transition temperature (T_c) [3]. As the transition takes place, electrical hysteresis loops appear spanning up to four orders of magnitude across regions near T_c [3].

Moreover, the amount of microwave response as a function of temperature is a convenient means to assess the electromagnetic properties of the studied VO_2 compounds [4], [5]. The change in conductivity leading to the phase transition arises from crystalline lattice deformations due to electron–phonon interactions driven by the temperature mechanism described by Peierls [6]. When VO_2 is introduced into substrates like sapphire, the temperature-dependent strain changes in the crystal structure transition cause the conduction of the film to increase or decrease during IMT.

From M_1 to R state, works [7], [8], [9] showed that single crystal VO_2 exhibit excellent IMT properties in contrast to the bulk polycrystalline VO_2 [9]. Polycrystalline VO_2 demonstrated IMT at a higher temperature compared to their thin film counterparts. The IMT at a lower temperature is due to the in-plane strain, from the lattice mismatch of the thin VO_2 sample and substrate [10], [11]. The IMT in VO_2 is attributed to two main mechanisms involving charge transport regimes: (i) The Mott transition, which is an electronic mechanism caused by electron-electron correlations [12] and, (ii) Peierls transition, a temperature-driven mechanism rising from crystalline lattice deformations due to electron–phonon interactions [5].

In [13], they showed a dielectric constant changing sign to negative using a complex dielectric function based on Lorentz-Drude dispersion. This theory describes frequency dependant polarization on bound charges based on reflection interactions between light and matter. In [14], the electrical conductivity is measured in DC while the dielectric property of VO_2 was extracted using the ABCD matrix and Nicolson-Ross-Weir (NRW) method. The ABCD matrix is used to separate the electromagnetic properties of VO_2 from its quartz substrate while NRW is used to extract the dielectric properties. The NRW uses the theory of plane wave incident on dielectric media to determine the complex permittivity and permeability [15]. In [16] the conductivity of VO_2 on sapphire was acquired from its imaginary dielectric constant using a similar approach to NRW. In [17] the real dielectric constant (ε'_{r,VO_2}) was extracted while the conductivity was measured at dc. Other works such as [18], [19], [20], and [21] similarly model VO_2 in the rf spectrum as a resistive material and conductivity was taken at the dc level.

Conductivity measurements carried out via electrodes in direct contact with VO_2 samples pose some issues. These measurements are not always repeatable and reliable due to factors such as surface discontinuity, grain boundaries, interfacial effects, and charge injection on the sample. The influence of the electrodes can be significantly reduced by confining the motion of the charge carriers into a smaller spatial area with the use of an electric field. Time-Resolved Microwave Conductivity (TRMC) is a measurement technique used to determine the conductivity of materials as a function of time. It quantifies charge carrier mobilities and dynamics for various semiconducting materials [22], [23]. TRMC is a contactless technique, which eliminates measurement deviations related to interfacial effects, discontinuous surfaces, grain boundaries and charge injections at the electrode-material interfaces, which otherwise complicate examination of fundamental material features, such as bulk charge carrier mobilities. Another merit is the lack of restrictions on the form of the material being measured, allowing samples ranging from single crystals and films to fluids and powders.

The Ka-band has been selected for use in the thin-film resonant microwave conductivity method due to its high frequency range for microwave transmission. This high frequency range provides a precise examination of the microwave conductivity of the samples, allowing for a thorough analysis of how the conductivity changes in response to microwave-transmitted power.

It is important to note that the method is not affected by frequency changes due to its spectroscopic nature. As the frequency of microwave transmission increases, the measurement sensitivity of the system also increases, resulting in a more precise examination of the sample's conductivity. On the other hand, utilizing lower frequencies may provide more comprehensive results as they may capture more detailed information about the conductivity of the sample at lower microwave-transmitted power levels.

The spectroscopic nature of the method enables a thorough analysis of the conductivity of the VO_2 thin films by utilizing the Ka-band. The results obtained from the method can be used to validate models and simulations, and to compare the conductivity of VO_2 with well-known materials such as Cu. The method also provides a valuable tool for studying the conductivity of thin film compounds and its dependence on frequency, making it a useful tool for understanding the electrical properties of materials for Frequency Selective Surface (FSS) applications.

VO_2-based FSS offers a high level of reconfigurability and versatility, making it a promising material for a wide range of applications [1]. The use of TRMC method as demonstrated in the study highlights the importance of understanding the material properties of VO_2 and similar materials for these applications such as chalcogenide glasses (GST) [24], liquid crystals [25], and graphene [26], [27] which exhibit unique electrical and thermal properties that can be used in FSS applications. It is important to note that while these materials may possess comparable attributes to VO_2, VO_2 has a distinct advantage due to its lower transition temperature, making it more suitable for specific applications [28].

One of the primary applications of VO_2-based FSS is in RF and microwave communication systems, where the FSS can be used as a dynamically reconfigurable filter [1], [28]. The FSS can switch between multiple states to selectively pass or block different frequency bands, making

it ideal for use in advanced communication systems that require bandwidth-efficient signal processing and frequency management.

Another application of VO_2-based FSS is in the field of smart antenna technology, where the FSS can be used to control the directivity of the antenna. The reconfigurable properties of the VO_2-based FSS make it ideal for use in smart antenna systems that require the ability to adapt to changing environments, such as those encountered in mobile communication systems [28]. In addition to communication systems, VO_2-based FSS can also be used in sensing applications, such as in the design of reconfigurable microwave sensors [29], [30], [31]. The ability to switch between multiple states allows the FSS to be used in a variety of sensing applications, such as in environmental monitoring, biomedical sensing, and security systems.

The VO_2-based FSS in [28] works by utilizing the reversible metal-insulator transition of VO_2 thin films. When an incident electromagnetic (EM) wave impinges on the FSS, the wave interacts with the VO_2 layer, causing a change in its conductivity. This change in conductivity affects the transmission response of the FSS to the incident wave.

In a conventional FSS, the transmission response is determined by the resonant frequencies of the metallic resonators and slots in the design [32]. However, in a VO_2-based FSS, the transmission response is dynamically reconfigurable and depends on the state of the VO_2 layer. If the VO_2 layer is in a high conductivity state, it acts as a metal and allows the incident wave to pass through, while if the VO_2 layer is in a low conductivity state, it acts as an insulator and blocks the wave.

In this paper, we report a TRMC study used for FSS applications on VO_2 compounds at 30 GHz. In these applications, the VO_2 layer is quickly and readily altered between its high and low conductivity states using external switching mechanisms like holographic storage [33] or lasers for optically imprinting reconfigurable patterns [28]. Due to the VO_2-based FSS's ability to dynamically adjust to variations in the incident wave's frequency, the transmission response is extremely adaptable and customizable.

The dynamics of thermally excited charged carriers have been monitored by observing the relationship between transmitted microwave power and conductivity using the sensitivity factor, in the waveguide and free space. Our investigations are focused on the thin film thickness of VO_2 screen printed on a 420 μm thick sapphire wafer with a circular diameter of 5 cm.

II. TIME-RESOLVED MICROWAVE CONDUCTANCE TECHNIQUE

In this TRMC analysis, temperature is used as a proxy for time, to examine the dynamic changes in the microwave conductivity of the samples. This is achieved by exposing the samples to microwave radiation and measuring their microwave conductivity as a function of temperature. In conventional Frequency Domain (FD) analysis, the material's conductivity is measured at different microwave frequencies, and a graph of conductivity vs frequency is produced [34].

One of the advantages of TRMC over Frequency Domain (FD) analysis to VO_2 material is that it provides a more comprehensive understanding of the material's conductivity as it changes with time. The temperature change in the material can be precisely controlled and monitored, providing a much more detailed picture of the material's conductive behavior over time [35]. This allows for a more accurate and in-depth analysis of the material's conductivity, including the detection of any changes in conductivity at specific temperatures, which may indicate changes in the material's microstructure or chemical composition [36].

Additionally, TRMC can provide a direct measurement of the material's conductivity, which is a key parameter in microwave engineering. Unlike FD analysis, which provides an indirect measurement of conductivity using complex mathematical models and assumptions, TRMC provides a more accurate and straightforward measurement of conductivity that is less prone to errors and inaccuracies [37].

When measuring the temperature-dependent electrical conductivity $\Delta\sigma(\mathrm{T})$ of the material, we use the Time-Resolved Microwave Conductivity (TRMC) method which was used in [23], [38], and [39] on photo-induced semiconducting samples. The method is based on spectroscopic analysis, whereby applying an external stimulus (such as light, temperature, or pressure) to the material as a function of time and observing the material perturbational response using spectrometric tools in this case high frequency microwaves [39]. The conductance of the material is evaluated by the change in power transmitted upon the application of heating in the form of smaller perturbations. In this work, the charge carriers are thermally generated using a low-power Peltier plate and the transport properties are probed using 30 GHz microwaves. The sample was thermally excited using a self-made thermoelectric assembly made up of a metal plate, heating element, heat sink and fan.

As the conductivity changes from σ to $\sigma + \Delta\sigma$ a change in the transmitted microwave power, $\Delta \mathrm{P}_t$, is observed. This leads to a change in the power transmission coefficient expressed as follows at a particular frequency:

$$\frac{\Delta P_t}{P_{in}} = \frac{P_t\,(\sigma + \Delta\sigma) + P_r\,(\sigma)}{P_{in}} = S_{21}\,(\sigma + \Delta\sigma) + S_{21}\,(\sigma) \tag{1}$$

where the transmission coefficient is expressed as $S_{21} = \mathrm{P}_t\,(\sigma)/\mathrm{P}_{\mathrm{in}}$. The relative change in transmitted microwave power is easier to obtain in terms of the steady-state unperturbed microwave power transmitted, $P_t\,(\sigma)$, as compared to the incident power, P_{in}, and is expressed elsewhere in [23], (1-4):

$$\frac{\Delta P_t}{P_t\,(\sigma)}\left(\frac{P_{in}^{-1}}{P_{in}^{-1}}\right) = \frac{S_{21}\,(\sigma + \Delta\sigma) + S_{21}\,(\sigma)}{S_{21}\,(\sigma)} \tag{2}$$

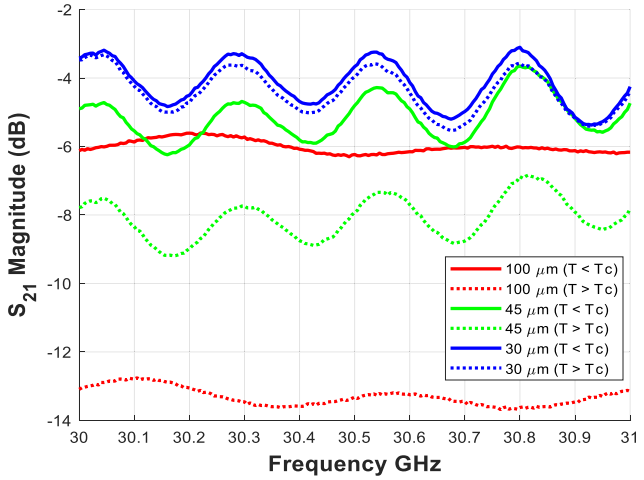

FIGURE 1. Measured transmission coefficient S_{21} of VO_2 sample at M_1 ($T < T_c$) and R ($T > T_c$) states as a function of frequency.

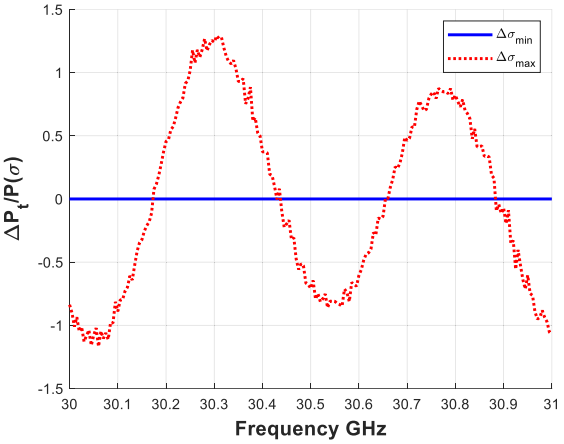

FIGURE 2. Normalized TRMC transients of VO_2 sample of 100 μm with minimum and maximum conductivities as a function of frequency.

Development of $S_{21}(\sigma + \Delta\sigma)$ in a Taylor series yield.

$$\frac{\Delta P_t}{P_t(\sigma)} = \frac{1}{S_{21}(\sigma)}\left(\frac{\delta S_{21}(\sigma)}{\delta\sigma}\right)_\sigma \Delta\sigma = A\Delta\sigma \tag{3}$$

where $\Delta\sigma$ is a tiny change as conductivity rises homogeneously from σ to $\sigma + \Delta\sigma$.

The *sensitivity factor* A is the ratio of the amount of power transmitted due to a change in the conductivity of the material. In general, the sensitivity factor measures how sensitive the microwave response of the sample is to changes in applied stimuli.

$$\begin{aligned} A &= \frac{S_{21}(\sigma + \Delta\sigma) + S_{11}(\sigma)/S_{21}(\sigma)}{\Delta\sigma} \\ &= \frac{1}{S_{21}(\sigma)}\left(\frac{\delta S_{21}(\sigma)}{\delta\sigma}\right)_\sigma \end{aligned} \tag{4}$$

Figure 1 shows the measured transmission coefficient at M_1 to R states of VO_2 samples of thickness 100, 45 and 30 μm. In the M_1 region, the samples are insulating, and the sample temperature, T, is less than T_c. While in the R region, where T is greater than T_c, the samples conduct and allow less transmission. Because the skin effect of the film is consistent across states, the thicker the films become, the more the phase transition occurs, resulting in increased conduction. The S_{21} of the 100, 45, and 30 μm films is -3, -5, and -6 dB in the M_1 state, respectively, while it is -3.5, -8, and -13 dB in the R state. The IMT attenuation of the 100 μm film is 7 dB, while that of the 45 and 30 μm films is 0.5 and 3 dB, respectively.

In the steady state, sensitivity factor A is positive. As $S_{21}(\sigma)$ falls, A tends to zero. In the range of σ where A changes signs, $\delta S_{21}(\sigma)$ becomes small and limits (7) [23]. A depends on the geometry and position of the sample in a system. It was formulated from microwave theory which is expressed as [39], (8-12):

$$A = \frac{1}{S_{21}(\sigma)}\frac{1}{2P_{in}}\iiint \times\left(\left|E_{(x,y,z,\sigma)}\right|^2 + \sigma\frac{\delta\left|E_{(x,y,z,\sigma)}\right|^2}{\delta\sigma}\right)dxdydz \tag{5}$$

Figure 2 shows the normalised TRMC transients of 100 μm VO_2 film with minimum and maximum conductivities contributions representing M_1 and R states respectively. The amplitude of the signal does not decay in the M_1 range because temperatures in this region ($T < T_c$) contribute only a small amount to IMT of higher modes of the signal. The peak amplitude of the signal varies with frequency in the R range due to changes in field strength inside the sample caused by temperature contributions associated with the effective conductivity of the sample.

A. EXPERIMENTAL ANALYSIS

The experimental setup shown in Figure 3 involves Ka-band waveguides, in which the sample is situated at the open ends of the waveguide system, resulting in a plane wave incident on the sample. The waveguides transmitted and reflected power is analyzed using an Agilent N5225A PNA system to determine the sample's properties. By subjecting the sample to conduction heating via a Peltier heating element located at the back of the sample, we monitored changes in microwave power. We specifically heated the sapphire layer from the z-direction, as illustrated in Figure 3(a). To understand how the sample's properties change with temperature, the sample's temperature is measured using K-type thermocouple contacts and a FLIR E5-XT thermal camera. The results showed that the perturbation-based approach allowed for the determination of the changes in the sample's microwave conductivity over time, providing a time-resolved measurement of the sample's properties.

In the measurement setup, a wave propagating along the z-axis in the TE_{10} waveguides in the x-y plane is terminated with the VO_2 films shown in Figure 3(b), and changes are monitored in the resonant response of the waveguide due to a perturbation of the sample material.

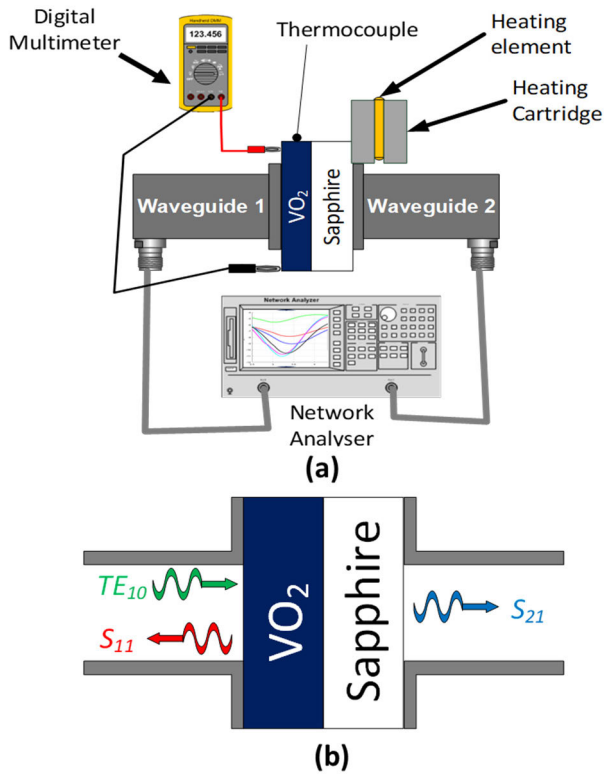

FIGURE 3. (a) Experimental schematic of setup with waveguide cavity demonstrating perturbation of VO_2 sample. (b) Schematic demonstrating plane wave incident on sample as s-parameters.

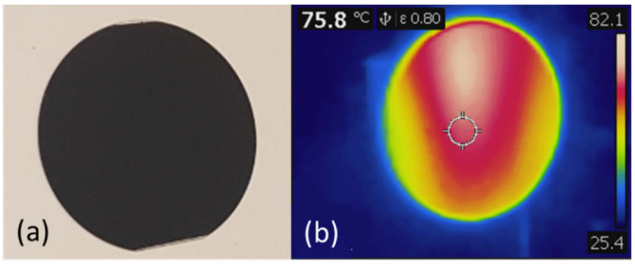

FIGURE 4. (a) Screen-printed VO_2 sample. (b) The thermal infrared image of the VO_2 sample with thermochromic properties. The thermal infrared image of the sample highlights the intensity vectors in color scale indicating heat distribution from 82.1 to 25.4 °C.

Figure 4a-b shows the sample under test. Sapphire thin film is used as a substrate to deposit VO_2 to perform the TRMC measurements. The substrate without VO_2 is used for measurement calibration, the S_{21} is ensured to be close to one as possible when the VO_2 is under room conditions. The sample is attached to the waveguide ends and clamped in place by the sample holder, allowing the distance between the sample and the short to be modified during calibration. The sample in Figure 3 is heated conductively through the sample holder from the back side of the film on the sapphire layer. Peltier elements are used to generate excitation, and heat flux sensors monitored the intensity of the excitation.

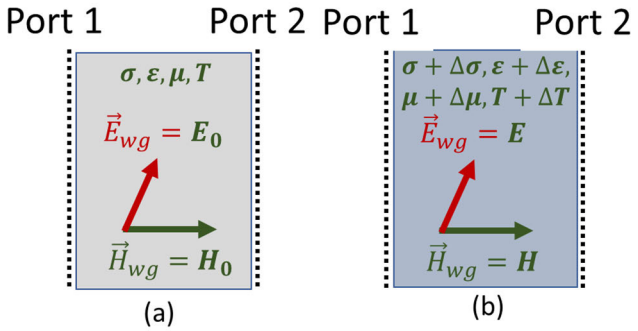

FIGURE 5. Perturbation of VO_2 sample in the waveguide (a) unperturbed sample state; (b) perturbed sample state.

Figure 5a represents a cross-section, S, of the unperturbed waveguide system with electric and magnetic fields E_0, H_0 and resonant frequency, ω_0, containing the VO_2 sample with an original conductivity, σ, perturbed permittivity, ε, unperturbed permeability, μ, Temperature, T. Figure 5b represents the same waveguide with the corresponding quantities E, H, ω after perturbation containing a transitioning VO_2 sample with its properties changed to $\sigma + \Delta\sigma$, $\varepsilon + \Delta\varepsilon$, $\mu + \Delta\mu$, $T + \Delta T$. Within S, the field equations applied as follows assuming the boundary is perfectly conducting:

In the initial case:

$$-\nabla \times E_0 = j\omega_0 \mu H_0 \tag{6}$$

$$\nabla \times H_0 = (\sigma + j\omega_0 \varepsilon) E_0 \tag{7}$$

For the transitioning case:

$$-\nabla \times E = j\omega (\mu + \Delta\mu) H \tag{8}$$

$$\nabla \times H = (\sigma + \Delta\sigma + j\omega\varepsilon + \Delta\varepsilon) E \tag{9}$$

Multiplying (9) by E_0 and H multiplied by conjugate of (8):

$$\iiint [\nabla \cdot (H \times E_0) - \nabla \cdot (H_0 \times E)]\, \delta V = \oiint \times (H \times E_0 - H_0 \times E)\, \delta S \tag{10}$$

On the surface, S:

$$\hat{n} \times E_0 = \hat{n} \times E = 0$$

$$0 = j(\omega - \omega_0) \iiint [\varepsilon E \cdot E_0 - \mu H \cdot H_0]\, dV + \iiint j\omega \left[\left(\Delta\varepsilon - \frac{j\Delta\sigma}{\omega} \right) E_0 \cdot E - \Delta\mu H \cdot H_0 \right] \times dV \tag{11}$$

$$\frac{\omega - \omega_0}{\omega} = \frac{-\iiint j\omega \left[\left(\Delta\varepsilon - \frac{j\Delta\sigma}{\omega} \right) E_0 \cdot E - \Delta\mu H \cdot H_0 \right] dV}{\iiint \left[\left(\varepsilon - \frac{j\sigma}{\omega} \right) E \cdot E_0 - \mu H \cdot H_0 \right] dV} \tag{12}$$

For a large transition which can be broken down into infinite small perturbations, we can replace E, H with the unperturbed field E_0, H_0. In a lossless case, the input impedance will be purely reactive. For lossy case the quality factor, Q, is high and the effect of dissipation can be considered by letting the resonant frequencies be complex [40]:

$$\omega \approx \omega_r + j\frac{\omega_0}{2Q} \tag{13}$$

$$\omega_r - \omega_0 + j\frac{\omega_0}{2Q} = \frac{-\omega_0 \iiint \left[\Delta\varepsilon \left|E_0\right|^2 - \Delta\mu \left|H_0\right|^2\right] dV}{\iiint \left[\varepsilon \left|E_0\right|^2 - \mu \left|H_0\right|^2\right] dV} + \frac{\iiint j\Delta\sigma \left|E_0\right|^2 dV}{\iiint \left[\varepsilon \left|E_0\right|^2 - \mu \left|H_0\right|^2\right] dV} \tag{14}$$

Assuming the electric and magnetic energies are equal:

$$\frac{\omega_0}{2Q} = \frac{\int\int\int \Delta\sigma \left|E_0\right|^2 dV}{2\int\int\int \varepsilon \left|E_0\right|^2 dV} \tag{15}$$

$$Q = \frac{\omega_0 \varepsilon}{\Delta\sigma} \tag{16}$$

In the waveguide configuration shown in Figure 3, the sensitivity factor A, assuming the change in the transmitted microwave is due to the sample absorption for normal uniform plane wave incidence on a homogeneous sample is expressed as (24) for dielectric medium [23], [41]

$$A_{\sigma_{min}} = -\frac{2k_0 k\imath - k_0 sin2k\imath}{k_0^2 + k^2 + \left(k^2 - k_0^2\right) cos2k\imath} \frac{2\omega\mu_0}{k} \tag{17}$$

and for a metallic medium where $S_{21}(\sigma) \approx 0$,

$$A_{\sigma_{max}} = \frac{2k_0 \left(\sqrt{A}_{\sigma_{\min}}\right)^3}{\sqrt{2\omega\mu_0}} \tag{18}$$

where $k_0 = \omega\sqrt{\mu_0\varepsilon_0}$ and $k = \omega\sqrt{\mu\varepsilon}$ are wave number of free space and thin film sample with thickness $\imath$, respectively. Wavenumber, k_s, is derived from [42](27) as:

$$cosk_s\imath = \frac{1 - S_{11}^2 + S_{21}^2}{2S_{21}} \tag{19}$$

the correction factor, $Corr(z)$, is derived as [43].

$$Corr(z) = \frac{\Delta P_{film}}{\Delta P_{cavity}} = \frac{2\imath}{d} \tag{20}$$

where d is the length of the waveguide. For samples that only partially fill the cavity cross-section, an extra correction factor must be used. as expressed, [43].

$$Corr(xy) = \frac{w}{ab}\left[w + \frac{a}{\pi} sin\left(\frac{\pi w}{a}\right)\right] \tag{21}$$

where a is the width of the waveguide, b is the height of the waveguide and w is the width of the sample. The modified cavity sensitivity factor $\tilde{A}$ for thin film samples are given as [43]:

$$\tilde{A} = Corr(z) \cdot Corr(xy) \cdot A \tag{22}$$

Figure 6 depicts the sensitivity factor of the system with various samples at 30 GHz as a function of temperature. A, for

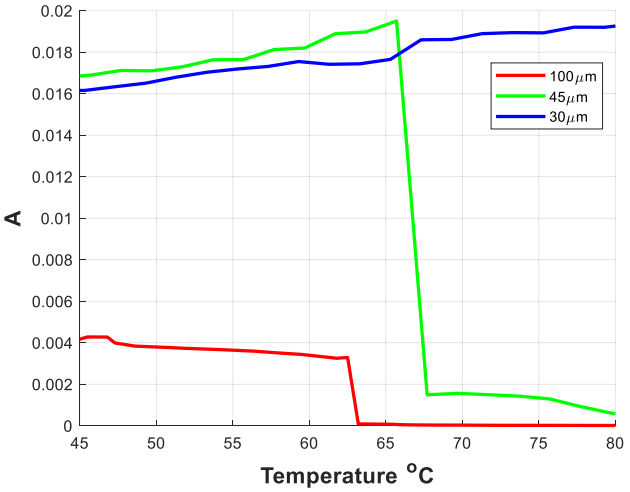

FIGURE 6. The sensitivity factor of the system at 30 GHz is a function of the temperature.

the 30 μm film stays slightly rises 0.016 to 0.019 throughout the temperature range, proving that there was no IMT in the sample. While the 100 μm film starts at 0.004 at M_1 and decreases to zero at the R region showing IMT, the 40 μm film has values of A like that of the 30 μm in the M_1 range, rising from 0.017 to 0.019 before decreasing to 0.002 and slightly declines across the R range. The two right-hand terms of (13) have the greatest influence on the sensitivity factor at the R range due to a decrease in microwave power transmission brought on by the weaker electric field within the sample.

The change in thickness of VO_2 has an impact on its electrical properties. The sensitivity factor of the system as a function of temperature is depicted in Figure 6, where the 30 μm film shows no insulator-to-metal transition (IMT), while the 40 μm and 100 μm films exhibit IMT, with the latter showing the most significant change. The steady-state microwave conductivity of the samples as a function of temperature change is shown in Figure 7, where the 45 μm film demonstrates similar kinetic activity to the 100 μm film, while the 30 μm film shows no change, further confirming the absence of IMT. The results indicate that the change in VO_2 thickness affects its electrical properties and therefore plays a role in the proposed methodology.

III. THERMOLYSIS TIME-RESOLVED MICROWAVE CONDUCTIVITY

In VO_2, the transition into the metallic state occurs due to the heating of the sample up to $T = T_c$ [44]. When free charge carriers are generated, they absorb microwaves which leads to a change in the microwave power [45], [37].

Using (4), we can find the change in conductivity ($\Delta\sigma$) as a function of time. $\Delta\sigma$ is associated with carrier localization on a Fermi level where different conduction mechanisms compete [46]. The reversible transition of VO_2 from a metal to an insulator involves the vanishing of the metallic conductivity σ_M at temperature $T = T_c$. The conductivity changes as a

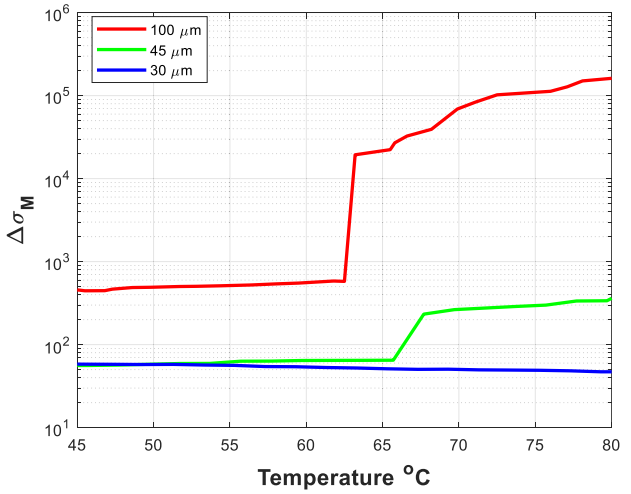

FIGURE 7. Steady-state microwave conductivity of sample materials as a function of temperature change.

function of temperature (T) are expressed as [47], (1-4):

$$\sigma_M(T) = \sigma_0(T) + \Delta\sigma(T) = \frac{ne^2\tau}{m} + mT^{\beta} \tag{23}$$

where, σ_0 is the original conductivity, e is the electron charge, m is the effective mass of charge carriers and $\beta = \left(e^3/\pi\varepsilon_r\varepsilon_0\right)^{1/2}$ is the Poole-Frenkel constant. The T^{β} term comes from Coulomb interactions.

The Coulomb interactions model with electron-electron and electron-hole scattering in the presence of random impurities predicts a $T^{1/2}$ correction to σ. [48], page 248:

$$\sigma_M(T) = \sigma_0(T) + mT^{\frac{1}{2}} + \beta T \tag{24}$$

The BT term arises from localization theory assuming an energy relaxation time τ_ε of the form $\frac{1}{\tau_\varepsilon} = cT^2$. Such a form is expected if the energy relaxation proceeds via electron-electron scattering. [49]. This is related to the sensitivity factor as [50]

$$A = -\frac{\tau_\varepsilon\left(1 + \frac{1}{\sqrt{S_{11}(\sigma)}}\right)}{\varepsilon} \tag{25}$$

where τ_ε, at resonance frequency is given as

$$\tau = \frac{Q}{\pi f_0} \tag{26}$$

Figure 7 depicts the microwave conductivity transient in the thin layers of the film. Higher modes contribute significantly to the TRMC signal in the *R* range due to the increased thickness above the skin effect that occurs at the excited surface in the 100 μm film. In the *R* range, microwave frequency modification does not affect the kinetics; only the signal amplitude is altered. As predicted by the theoretical analysis, the same kinetic activity was observed in the transitioning 45 μm film. In the 30 μm film, no change is observed further verifying the lack of IMT.

IV. VALIDATION OF RESULTS

The validity of this result in Figure 7 from (3) was determined by obtaining the conductivity of the films and replicating the plane wave incident on medium conditions shown in Figure 5 in the CST simulation environment by altering the conductivity as a function of temperature.

In VO_2, the transport of charge and heat currents were observed to be by separate diffusive modes rather than quasiparticles [51]. This causes a violation of the Wiedemann-Franz (WF) law near the IMT region [52]. WF shows the sum of a metal's electrical conductivity (σ), and absolute temperature (T) determines the metal's thermal conductivity (k_e). The constant relating them is the Lorenz number (L), which is equal to the Sommerfeld value, $L_0 = \frac{\pi^2}{3}\left(\frac{k_e}{e}\right)^2$, these conditions are satisfied predominantly for elastic scattering [53]. In VO_2, the deviation of L away from L_0 is attributed to a breakdown in inelastic electron interactions in the quasiparticle Drude model, which scatters conduction electrons. Reference [53] showed that the presence of point defects scatters electrons elastically to restore the Lorenz number toward the Sommerfeld value. Point defects are the vacancies and interstitials of V and O atoms. The transient conductance is related k_e as follows:

$$\Delta\sigma_M = \frac{\Delta G_M b}{at} = \frac{k_e}{L\Delta T} \tag{27}$$

Figure 8 shows the measured and simulated transient conductance of the films. The values were input into the CST environment to produce the transmission response of the film. The maximum change in conductivity was extracted from changing temperature measurements. The net yield of mobile charge carriers was not known for our VO_2 sample; however, it was assumed to be smaller than or equal to 1.

At T < T_c, the TRMC signal is assumed to be at maximum. The product $\phi_{max(\Delta T)}\Sigma\mu$ corresponds to values that are slightly like the actual electrical mobility of the charge carrier values., this assessment is valid for short time scales, where $\phi_{(\Delta T)} = \phi_{max} = 1$ [54].

The experimental setup illustrated in Figure 9(a) is based on the concept of plane waves on dielectric media. Plane waves are electromagnetic waves that have a uniform wavefront and propagate in a straight line. In a dielectric medium, such as the sample being simulated, the wave velocity is lower than the velocity of light in a vacuum. The ratio of the two velocities is known as the refractive index, which is a material property that characterizes how much the medium retards the propagation of the electromagnetic wave [55].

In the simulation show in Figure 9(b), the CST Microwave Studio software generates a plane wave that propagates through a volume containing layers of VO_2 and sapphire with a small air gap in between. The wave is excited using waveguide ports of linear polarization. These ports can be used to mimic the incident plane wave over the sample under test. In particular, the waveguide ports generate an electromagnetic field that is uniform in the transverse plane and that has a linear polarization. The wave port is an

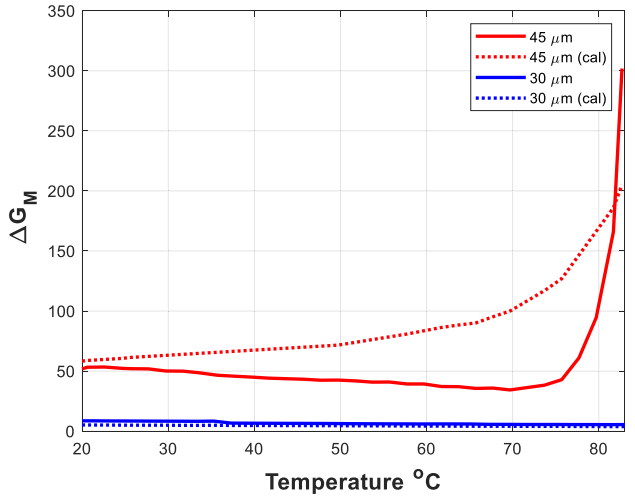

FIGURE 8. Measured and simulated transient conductance of films as a function of temperature.

electromagnetic boundary condition that mimics the incident plane wave over the sample under test. The wave port is placed at the edge of the simulation domain and serves as a source of the incident electromagnetic field. It is designed to provide the correct amplitude, phase, and polarization of the incident wave. This field is used to excite the plane wave in the simulation.

The transient conductance of the films is parameterized as a function of temperature. This parameterization is necessary to enable the calculation of the transmission coefficient for a range of temperatures. The simulation is performed using the frequency domain solver at a frequency of 30 GHz. VO_2 is modelled as a ''normal material'' since the electrical conductance is adjusted based on the calculated values. This simulation setup allows for the investigation of the transmission properties of the VO_2 sample as a function of temperature, providing insights into the changes in the microwave conductivity of the sample observed over time.

To ensure the reliability and accuracy of our results in studying the microwave transmission characteristics of VO_2, the temperature probe is carefully calibrated using a calibrated thermometer with accuracy of 2%. A thermal imaging camera is used to verify the probe data, which provided a visual representation of the sample's temperature distribution and helped us to further ensure the accuracy of our results.

The samples are heated, and multiple runs of the experiment were performed at different temperatures to obtain a range of temperature readings. Averaging these runs enabled us to estimate the uncertainty associated with the temperature measurements, which is critical in assessing the reliability of our findings. Moreover, we took measures to ensure that the sample reached temperature equilibrium during heating, this involved allowing sufficient time for the sample to equilibrate at each temperature which helped to reduce sources of experimental error.

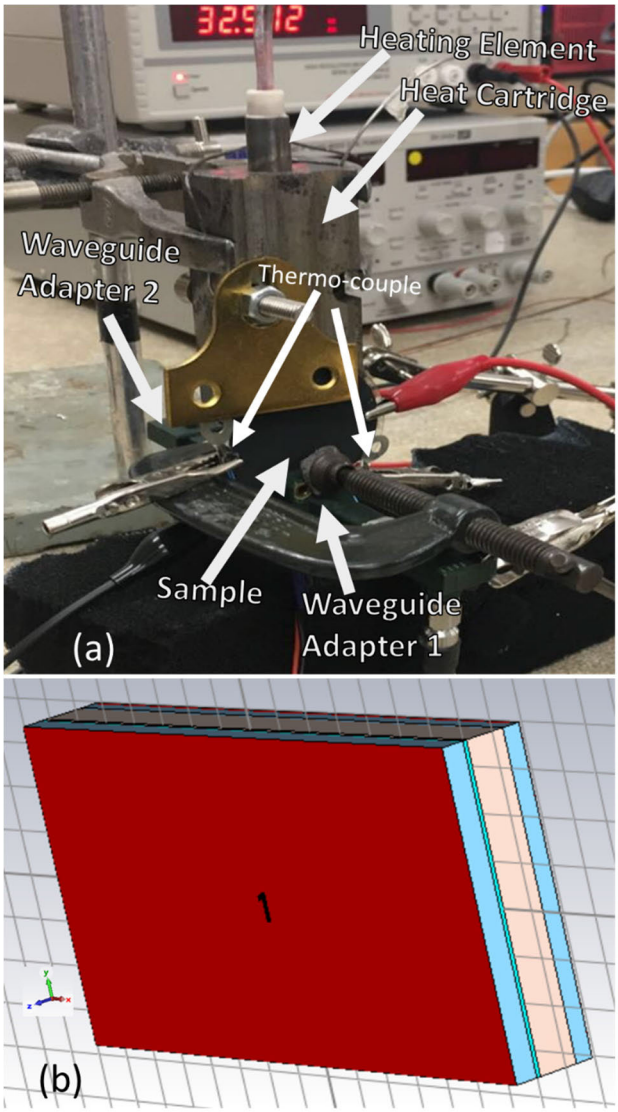

FIGURE 9. Plane-wave incidence. (a) Experimental setup of Figure 3. (b) CST studio environment with waveguide ports (in red) was used to mimic plane waves with the sample (grey for sapphire and black for VO_2) with air gaps in light blue.

In addition, the algorithm used during the measurements were modified to account for possible sources of inaccuracy such as sample thickness, homogeneity, and temperature variations as shown in (19). This helped to improve the accuracy of our temperature measurements. The overall uncertainty in our temperature measurements is 3°C.

By changing the transient conductance values from Figure 8, Figure 10 displays the measured and simulated transmission response of the films. The measured response of the films and their simulation are in good agreement. While the 45 μm gradually attenuates from -5 dB, the 30 μm shows no transition at that level. With a 7 dB attenuation, the 100 μm is the most conductive. Further validation was done by measuring a Cu wafer and comparing the extracted values with other works in [56], [57], and [58] with the results in close agreement as shown in Figure 11.

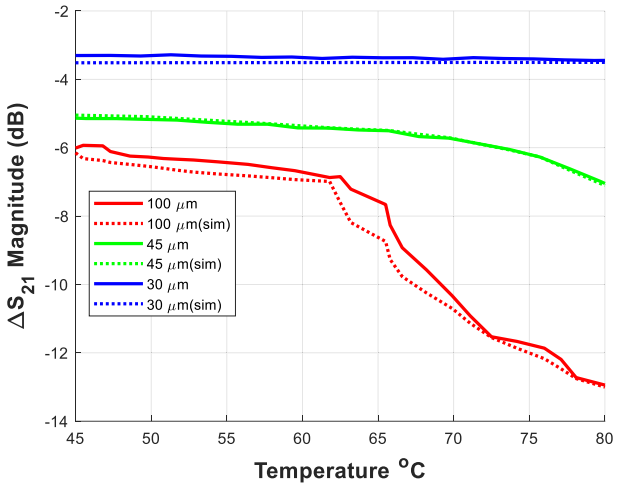

FIGURE 10. Measured and simulated transmission coefficient (S_{21}) of VO_2 samples at 30 GHz across temperature.

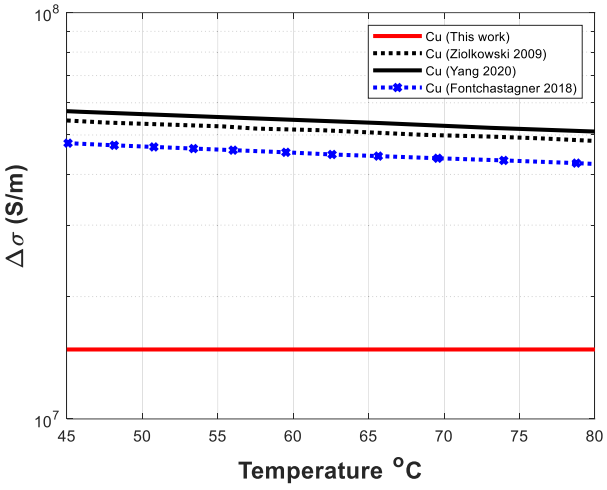

FIGURE 11. Measured transient microwave conductivity of Cu across temperature compared with other recent literature results: Ziolkowski 2009 [56], Fontchastagner 2018 [57] and Yang 2020 [58].

V. CONCLUSION

We have presented a contactless TRMC study on VO_2 films that provide a substitute for dc/ac electrical measurements made between electrodes. This technique showed how the microwave conductivity of thermally excited VO_2 samples changes in response to microwave transmission power. This is observed through the sensitivity factor of the system that uses Ka-band microwave waveguides. The sensitivity factor was derived from the electromagnetic field study on perturbation analysis of the medium in the waveguide for 2 cases representing the various states of VO_2 during the transition.

We used ways to validate the method. Firstly, we demonstrate that the CST simulation fits the experimental results of the transmission coefficient with a single set of material parameters for the sapphire substrate and the waveguide components using a series of tests with VO_2 films of various thicknesses. Secondly, the extracted conductivities of the thin films of copper closely match those of earlier works in the literature.

TRMC experiments show a low mode in microwave conductivity below the T_c of VO_2, which is close to 65°C, in agreement with the dielectric properties of the charge carriers. This is consistent with shallow trap electron states being real. Longer electron hops increase the barrier energy at T_c, where these states are exothermic, resulting in a microwave conduction mode that is triggered by heat.

Moreover, the use of temperature as a proxy for time in TRMC analysis provides a more detailed and accurate understanding of the material's conductive behavior compared to traditional FD analysis. This makes TRMC a powerful tool for investigating the conductive properties of materials for a wide range of applications, including those in the field of microwave engineering and technology.

REFERENCES

[1] D. E. Anagnostou, D. Torres, T. S. Teeslink, and N. Sepulveda, "Vanadium dioxide for reconfigurable antennas and microwave devices: Enabling RF reconfigurability through smart materials," *IEEE Antennas Propag. Mag.*, vol. 62, no. 3, pp. 58–73, Jun. 2020, doi: 10.1109/MAP.2020.2964521.

[2] Z. Shao, X. Cao, H. Luo, and P. Jin, "Recent progress in the phase-transition mechanism and modulation of vanadium dioxide materials," *NPG Asia Mater.*, vol. 10, no. 7, pp. 581–605, Jul. 2018, doi: 10.1038/s41427-018-0061-2.

[3] D. E. Anagnostou, T. S. Teeslink, D. Torres, and N. Sepulveda, "Vanadium dioxide reconfigurable slot antenna," in *Proc. IEEE Int. Symp. Antennas Propag. (APSURSI)*, Jun. 2016, pp. 1055–1056, doi: 10.1109/APS.2016.7696235.

[4] E. Caruthers and L. Kleinman, "Energy bands of semiconducting VO_2," *Phys. Rev. B, Condens. Matter*, vol. 7, no. 8, pp. 3760–3766, Apr. 1973, doi: 10.1103/PhysRevB.7.3760.

[5] R. M. Wentzcovitch, W. W. Schulz, and P. B. Allen, "VO_2: Peierls or Mott–Hubbard? A view from band theory," *Phys. Rev. Lett.*, vol. 72, no. 21, pp. 3389–3392, May 1994, doi: 10.1103/PhysRevLett.72.3389.

[6] T. M. Rice, H. Launois, and J. P. Pouget, "Comment on 'VO_2: Peierls or Mott–Hubbard? A view from band theory,'" *Phys. Rev. Lett.*, vol. 73, no. 22, p. 3042, Nov. 1994, doi: 10.1103/PHYSREVLETT.73.3042.

[7] C. Zhao, S. Ma, Z. Li, W. Li, J. Li, Q. Hou, and Y. Xing, "Simple and fast fabrication of single crystal VO_2 microtube arrays," *Commun. Mater.*, vol. 1, no. 1, pp. 1–9, May 2020, doi: 10.1038/s43246-020-0031-4.

[8] K. Liu, S. Lee, S. Yang, O. Delaire, and J. Wu, "Recent progresses on physics and applications of vanadium dioxide," *Mater. Today*, vol. 21, no. 8, pp. 875–896, Oct. 2018, doi: 10.1016/J.MATTOD.2018.03.029.

[9] R. Shi, N. Shen, J. Wang, W. Wang, A. Amini, N. Wang, and C. Cheng, "Recent advances in fabrication strategies, phase transition modulation, and advanced applications of vanadium dioxide," *Appl. Phys. Rev.*, vol. 6, no. 1, Mar. 2019, Art. no. 011312, doi: 10.1063/1.5087864.

[10] P. Jin, K. Yoshimura, and S. Tanemura, "Dependence of microstructure and thermochromism on substrate temperature for sputter-deposited VO_2 epitaxial films," *J. Vac. Sci. Technol. A, Vac., Surf., Films*, vol. 15, no. 3, pp. 1113–1117, May 1997, doi: 10.1116/1.580439.

[11] R. M. Bowman and J. M. Gregg, "VO_2 thin films: Growth and the effect of applied strain on their resistance," *J. Mater. Sci., Mater. Electron.*, vol. 9, pp. 187–191, Jun. 1998, doi: 10.1023/A:1008822023407.

[12] A. Zylbersztejn and N. F. Mott, "Metal-insulator transition in vanadium dioxide," *Phys. Rev. B, Condens. Matter*, vol. 11, pp. 4383–4395, Jun. 1975, doi: 10.1103/PhysRevB.11.4383.

[13] J. B. K. Kana, G. Vignaud, A. Gibaud, and M. Maaza, "Thermally driven sign switch of static dielectric constant of VO_2 thin film," *Opt. Mater.*, vol. 54, pp. 165–169, Apr. 2016, doi: 10.1016/J.OPTMAT.2016.02.032.

[14] B. J. Mapleback, K. J. Nicholson, M. Taha, T. C. Baum, and K. Ghorbani, "Complex permittivity and permeability of vanadium dioxide at microwave frequencies," *IEEE Trans. Microw. Theory Techn.*, vol. 67, no. 7, pp. 2805–2811, Jul. 2019, doi: 10.1109/TMTT.2019.2916824.

[15] E. J. Rothwell, J. L. Frasch, S. M. Ellison, P. Chahal, and R. O. Ouedraogo, "Analysis of the Nicolson–Ross–Weir method for characterizing the electromagnetic properties of engineered materials," *Prog. Electromagn. Res.*, vol. 157, pp. 31–47, 2016, doi: 10.2528/pier16071706.

[16] N. J. Estes and J. D. Chisum, "Increased power handling of vanadium dioxide T/R switches using a resonant topology," in *IEEE MTT-S Int. Microw. Symp. Dig.*, Jun. 2019, pp. 669–672, doi: 10.1109/MWSYM.2019.8701088.

[17] E. A. Casu, A. M. Ionescu, N. Oliva, M. Cavalieri, A. A. Muller, A. Fumarola, W. A. Vitale, A. Krammer, A. Schuler, and M. Fernandez-Bolanos, "Tunable RF phase shifters based on vanadium dioxide metal insulator transition," *IEEE J. Electron Devices Soc.*, vol. 6, pp. 965–971, 2018, doi: 10.1109/JEDS.2018.2837869.

[18] Y. Zhou and S. Ramanathan, "Mott memory and neuromorphic devices," *Proc. IEEE*, vol. 103, no. 8, pp. 1289–1310, Aug. 2015, doi: 10.1109/JPROC.2015.2431914.

[19] Y. Zhou, X. Chen, C. Ko, Z. Yang, C. Mouli, and S. Ramanathan, "Voltage-triggered ultrafast phase transition in vanadium dioxide switches," *IEEE Electron Device Lett.*, vol. 34, no. 2, pp. 220–222, Feb. 2013, doi: 10.1109/LED.2012.2229457.

[20] W. Li, M. Vaseem, S. Yang, and A. Shamim, "Flexible and reconfigurable radio frequency electronics realized by high-throughput screen printing of vanadium dioxide switches," *Microsyst. Nanoeng.*, vol. 6, no. 1, pp. 1–12, Oct. 2020, doi: 10.1038/s41378-020-00194-2.

[21] G. Zhang, H. Ma, C. Lan, R. Gao, and J. Zhou, "Microwave tunable metamaterial based on semiconductor-to-metal phase transition," *Sci. Rep.*, vol. 7, no. 1, pp. 1–6, Jul. 2017, doi: 10.1038/s41598-017-06230-y.

[22] J. Dugay, W. Evers, R. Torres-Cavanillas, M. Giménez-Marqués, E. Coronado, and H. S. J. Van der Zant, "Charge mobility and dynamics in spin-crossover nanoparticles studied by time-resolved microwave conductivity," *J. Phys. Chem. Lett.*, vol. 9, no. 19, pp. 5672–5678, Oct. 2018, doi: 10.1021/ACS.JPCLETT.8B02267.

[23] M. Kunst and G. Beck, "The study of charge carrier kinetics in semiconductors by microwave conductivity measurements," *J. Appl. Phys.*, vol. 60, no. 10, pp. 3558–3566, Nov. 1986, doi: 10.1063/1.337612.

[24] F. Ding, Y. Yang, and S. I. Bozhevolnyi, "Dynamic metasurfaces using phase-change chalcogenides," *Adv. Opt. Mater.*, vol. 7, no. 14, Jul. 2019, Art. no. 1801709, doi: 10.1002/ADOM.201801709.

[25] A. P. Gregory and R. N. Clarke, "A review of RF and microwave techniques for dielectric measurements on polar liquids," *IEEE Trans. Dielectr. Electr. Insul.*, vol. 13, no. 4, pp. 727–743, Aug. 2006, doi: 10.1109/TDEI.2006.1667730.

[26] X. Li, C. Ma, J. Yu, B. Xiao, L. Xiao, and X. Wang, "Dynamically tunable broadband absorber/reflector based on graphene and VO_2 metamaterials," *Appl. Opt.*, vol. 61, no. 7, pp. 1646–1651, Mar. 2022, doi: 10.1364/AO.448619.

[27] Y. Luo, Q. Zeng, X. Yan, Y. Wu, Q. Lu, C. Zheng, N. Hu, W. Xie, and X. Zhang, "Graphene-based multi-beam reconfigurable THz antennas," *IEEE Access*, vol. 7, pp. 30802–30808, 2019, doi: 10.1109/ACCESS.2019.2903135.

[28] Q. Abdullahi, A. Dzipalski, C. Raguenes, N. Sepulveda, G. Jose, A. Shanim, G. Goussetis, D. Hand, and D. E. Anagnostou, "Use of thermochromic properties of VO_2 for reconfigurable frequency selection," *Electronics*, vol. 11, no. 24, p. 4099, Dec. 2022, doi: 10.3390/electronics11244099.

[29] E. Strelcov, Y. Lilach, and A. Kolmakov, "Gas sensor based on metal-insulator transition in VO_2 nanowire thermistor," *Nano Lett.*, vol. 9, no. 6, pp. 2322–2326, Jun. 2009, doi: 10.1021/nl900676n.

[30] B.-J. Kim, Y. W. Lee, B.-G. Chae, S. J. Yun, S.-Y. Oh, H.-T. Kim, and Y.-S. Lim, "Temperature dependence of the first-order metal-insulator transition in VO_2 and programmable critical temperature sensor," *Appl. Phys. Lett.*, vol. 90, no. 2, Jan. 2007, Art. no. 023515, doi: 10.1063/1.2431456.

[31] S. Chen, H. Ma, X. Yi, T. Xiong, H. Wang, and C. Ke, "Smart VO_2 thin film for protection of sensitive infrared detectors from strong laser radiation," *Sens. Actuators A, Phys.*, vol. 115, no. 1, pp. 28–31, Sep. 2004, doi: 10.1016/J.SNA.2004.03.018.

[32] B. Munk, "Frequency selective surfaces: Theory and design [book review]," *IEEE Signal Process. Mag.*, vol. 18, no. 1, p. 94, Jan. 2001, doi: 10.1109/msp.2001.911199.

[33] W. R. Roach, "Holographic storage in VO_2," *Appl. Phys. Lett.*, vol. 19, no. 11, pp. 453–455, Dec. 1971, doi: 10.1063/1.1653769.

[34] A. F. Peterson and S. P. Castillo, "A frequency-domain differential equation formulation for electromagnetic scattering from inhomogeneous cylinders," *IEEE Trans. Antennas Propag.*, vol. AP-37, no. 5, pp. 601–607, May 1989, doi: 10.1109/8.24188.

[35] A. F. Peterson and S. P. Castillo, "A frequency-domain differential equation formulation for electromagnetic scattering from inhomogeneous cylinders," *IEEE Trans. Antennas Propag.*, vol. 37, no. 5, pp. 601–607, May 1989, doi: 10.1109/8.24188.

[36] G. L. Sorger, J. P. Oliveira, P. L. Inácio, N. Enzinger, P. Vilaça, R. M. Miranda, and T. G. Santos, "Non-destructive microstructural analysis by electrical conductivity: Comparison with hardness measurements in different materials," *J. Mater. Sci. Technol.*, vol. 35, no. 3, pp. 360–368, Mar. 2019, doi: 10.1016/j.jmst.2018.09.047.

[37] O. G. Reid, D. T. Moore, Z. Li, D. Zhao, Y. Yan, K. Zhu, and G. Rumbles, "Quantitative analysis of time-resolved microwave conductivity data," *J. Phys. D, Appl. Phys.*, vol. 50, no. 49, Nov. 2017, Art. no. 493002, doi: 10.1088/1361-6463/AA9559.

[38] G. Beck and M. Kunst, "Contactless scanner for photoactive materials using laser-induced microwave absorption," *Rev. Sci. Instrum.*, vol. 57, no. 2, pp. 197–201, Feb. 1986, doi: 10.1063/1.1138968.

[39] M. Kunst and G. Beck, "The study of charge carrier kinetics in semiconductors by microwave conductivity measurements. II," *J. Appl. Phys.*, vol. 63, no. 4, pp. 1093–1098, Feb. 1988, doi: 10.1063/1.340013.

[40] R. F. Harrington, *Time-Harmonic Electromagnetic Fields*. IEEE Press, 2001, doi: 10.1109/9780470546710.

[41] S. Arslanagic, T. V. Hansen, N. A. Mortensen, A. H. Gregersen, O. Sigmund, R. W. Ziolkowski, and O. Breinbjerg, "A review of the scattering-parameter extraction method with clarification of ambiguity issues in relation to metamaterial homogenization," *IEEE Antennas Propag. Mag.*, vol. 55, no. 2, pp. 91–106, Apr. 2013, doi: 10.1109/MAP.2013.6529320.

[42] S. Arslanagić, T. V. Hansen, N. A. Mortensen, A. H. Gregersen, O. Sigmund, R. W. Ziolkowski, and O. Breinbjerg, "A review of the scattering-parameter extraction method with clarification of ambiguity issues in relation to metamaterial homogenization," *IEEE Antennas Propag. Mag.*, vol. 55, no. 2, pp. 91–106, Apr. 2013, doi: 10.1109/MAP.2013.6529320.

[43] G. Dicker, *Photogeneration and Dynamics of Charge Carriers in the Conjugated Polymer Poly(3-Hexylthiophene)*. Delft, The Netherlands: Delft Univ. Press, 2004.

[44] F. A. Chudnovskii, "Metal-semiconductor phase transition in vanadium oxides and technical applications," *Zhurnal Tekhnicheskoi Fiziki*, vol. 45, pp. 1561–1583, Aug. 1975.

[45] J. M. Schins and E. Talgorn, "Conductive response of a photo-excited sample in a radio-frequent driven resonance cavity," *Rev. Sci. Instrum.*, vol. 82, no. 6, Jun. 2011, Art. no. 064703, doi: 10.1063/1.3600062.

[46] A. G. Zabrodskii, "Coulomb gap, its critical behavior, and the metal-insulator transition in doped semiconductors," *Czechoslovak J. Phys.*, vol. 46, no. S5, pp. 2455–2456, May 1996, doi: 10.1007/BF02570214.

[47] V. F. Gantmakher, "Effect of the Coulomb interaction on the electron energy spectrum," in *Electrons and Disorder in Solids* (International Series of Monographs on Physics), L. I. Man, Ed. Oxford, U.K.: Oxford Univ. Press, Aug. 2005, pp. 43–57.

[48] W.S.B, "Electron-electron interactions in disordered systems: Edited by A. L. Efros and M. Pollak. North-Holland, Amsterdam, 1985. 690 pages," *J. Magn. Reson. (1969)*, vol. 79, no. 1, p. 219, 1988.

[49] A. Pergament, A. Crunteanu, A. Beaumont, G. Stefanovich, and A. Velichko, "Vanadium dioxide: Metal-insulator transition, electrical switching and oscillations. A review of state of the art and recent progress," Jan. 2016, *arXiv:1601.06246*.

[50] J. M. Warmax, P. P. Infelta, M. P. De Haas, and A. Hummel, "The study of primary and secondary charge carriers in nanosecond pulse irradiated liquid dielectrics using a resonant microwave cavity," *Can. J. Chem.*, vol. 55, pp. 2249–2257, Jul. 1977.

[51] S. S. N. Bharadwaja, C. Venkatasubramanian, N. Fieldhouse, S. Ashok, M. W. Horn, and T. N. Jackson, "Low temperature charge carrier hopping transport mechanism in vanadium oxide thin films grown using pulsed DC sputtering," *Appl. Phys. Lett.*, vol. 94, no. 22, Jun. 2009, Art. no. 222110, doi: 10.1063/1.3139864.

[52] S. Lee, K. Hippalgaonkar, F. Yang, J. Hong, C. Ko, J. Suh, K. Liu, K. Wang, J. J. Urban, X. Zhang, C. Dames, S. A. Hartnoll, O. Delaire, and J. Wu, "Anomalously low electronic thermal conductivity in metallic vanadium dioxide," *Science*, vol. 355, no. 6323, pp. 371–374, Jan. 2017, doi: 10.1126/science.aag0410.

[53] L. Jin, S. E. Zeltmann, H. S. Choe, H. Liu, F. I. Allen, A. M. Minor, and J. Wu, "Disorder recovers the Wiedemann–Franz law in the metallic phase of VO2," *Phys. Rev. B, Condens. Matter*, vol. 102, no. 4, Jul. 2020, Art. no. 041120, doi: 10.1103/PHYSREVB.102.041120.

[54] M. Rini, Z. Hao, R. W. Schoenlein, C. Giannetti, F. Parmigiani, S. Fourmaux, J. C. Kieffer, A. Fujimori, M. Onoda, S. Wall, and A. Cavalleri, "Optical switching in VO_2 films by below-gap excitation," *Appl. Phys. Lett.*, vol. 92, no. 18, May 2008, Art. no. 181904, doi: 10.1063/1.2921784.

[55] D. Pozar, *Microwave Engineering*, 4th ed. New York, NY, USA: Wiley, 2011.

[56] M. Ziolkowski and H. Brauer, "Modelling of Seebeck effect in electron beam deep welding of dissimilar metals," *COMPEL-Int. J. Comput. Math. Electr. Electron. Eng.*, vol. 28, no. 1, pp. 140–153, Jan. 2009, doi: 10.1108/03321640910918940.

[57] J. Fontchastagner, T. Lubin, S. Mezani, and N. Takorabet, "Design optimization of an axial-field eddy-current magnetic coupling based on magneto-thermal analytical model," *Open Phys.*, vol. 16, no. 1, pp. 21–26, Mar. 2018, doi: 10.1515/phys-2018-0004.

[58] P. Yang, S. Dai, T. Ma, J. Huang, G. Jiang, Y. Wang, Z. Hong, and Z. Jin, "Analysis of peak electromagnetic torque characteristics for superconducting DC induction heaters," *IEEE Access*, vol. 8, pp. 14777–14788, 2020, doi: 10.1109/ACCESS.2019.2963718.

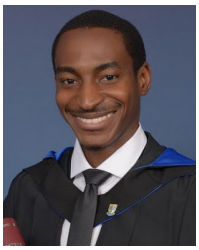

QASSIM ABDULLAHI (Student Member, IEEE) received the M.Eng. degree (Hons.) in electrical and electronics engineering and the Ph.D. degree from Heriot-Watt University, Edinburgh, U.K., in 2018 and 2023, respectively. In 2016, he joined Samsung Group, Edinburgh, as a RF Engineer for far field wireless power transfer. Between 2017 and 2018, he worked with Feel the Warmth in collaboration with Scottish Enterprise, Edinburgh, as a System Engineer. In 2019, he joined the Institute of Signals, Sensors, and Systems (ISSS), Heriot-Watt University, as a Researcher. His research interests include compact wearable antennas, frequency selective surface, metamaterials, wearable antennas, phase changing materials, and wireless power transfer.

MOHAMMAD VASEEM (Member, IEEE) received the M.Sc. degree in physical chemistry from Aligarh Muslim University, Aligarh, India, in 2005, and the Ph.D. degree in chemical engineering from Chonbuk National University, Jeonju, South Korea, in 2011. From 2011 to 2014, he was a Post-Doctoral Fellow with World Class University Project and Brain Korea 21 Project with Chonbuk National University. From 2015 to 2018, he was a Post-Doctoral Fellow with the Electrical Engineering Program with the King Abdullah University of Science and Technology, Thuwal, Saudi Arabia, where he is currently a Research Scientist. He has more than 12 years of experience in material preparation and ink-formulation for printed electronics. For the last six years, his focus has been on functional ink-materials for RF electronics and sensor. He has developed magnetic and VO2-based ink-materials for fully printed reconfigurable and tunable applications. He has authored more than 60 publications, three book chapters, five patents, and 80 research paper presentations in several national and international conferences.

ATIF SHAMIM (Senior Member, IEEE) received the M.S. and Ph.D. degrees in electrical engineering from Carleton University, Ottawa, ON, Canada, in 2004 and 2009, respectively. He was an NSERC Alexander Graham Bell Graduate Scholar with Carleton University from 2007 to 2009 and an NSERC Post-Doctoral Fellow in 2009 to 2010 with Royal Military College Canada and the King Abdullah University of Science and Technology (KAUST), Thuwal, Saudi Arabia. In August 2010, he joined the Electrical Engineering Program, KAUST, where he is currently an Associate Professor and Principal investigator of the IMPACT Laboratory. He was an Invited Researcher with the VTT Micro-Modules Research Center, Oulu, Finland, in 2006. He is an author of one book, three book chapters, and 250 publications; an inventor on 30 patents; and has given 70 invited talks at various international forums. His research interests include innovative antenna designs and their integration strategies with circuits and sensors for flexible and wearable wireless sensing systems through a combination of CMOS and additive manufacturing technologies. He is a Member of the IEEE APS Measurements Committee and the IEEE MTT Microwave Control Techniques Committee, founded the first IEEE AP/MTT chapter in Saudi Arabia (2013) and served an Editorial Board of IEEE Transactions on Antennas and Propagation (2013 to 2019), and as the Guest Editor for IEEE AWPL Special issue (2019). He is currently an Associate Editor for IEEE Journal of Electromagnetics, RF and Microwaves in Medicine and Biology. He was the recipient of best paper awards in IEEE IMS 2016, IEEE MECAP 2016, IEEE EuWiT 2008; first prize in the IEEE IMS 2019 3MT competition; finalist/honorable mention prizes in IEEE APS Design Competition 2020, IEEE APS 2005, IEEE IMS 2014, IEEE IMS 2017 (3MT competition); and R. W. P. King IEEE Award for journal papers in IEEE TAP 2017 and 2020. He was given the Ottawa Centre of Research Innovation (OCRI) Researcher of the Year Award in 2008 in Canada. His work on wireless dosimeter won the ITAC SMC Award at Canadian Microelectronics TEXPO in 2007. He was the recipient of numerous business-related awards, including 1st Prize in Canada's national business plan competition and was awarded OCRI Entrepreneur of the Year Award in 2010 and the Kings Prize for the best innovation of the year (2018) for his work on sensors for the oil industry.

GEORGE GOUSSETIS (Senior Member, IEEE) received the Diploma degree in electrical and computer engineering from the National Technical University of Athens, Greece, in 1998, the B.Sc. degree (Hons.) in physics from University College London (UCL), London, U.K., in 2002, and the Ph.D. degree from the University of Westminster, London, in 2002. In 1998, he joined Space Engineering, Rome, Italy, as a RF Engineer. In 1999, he was with the Wireless Communications Research Group, University of Westminster, as a Research Assistant. From 2002 to 2006, he was a Senior Research Fellow with Loughborough University, U.K. Between 2006 and 2009, he was a Lecturer (an Assistant Professor) with the School of Engineering and Physical Sciences, Heriot-Watt University, Edinburgh, U.K. He joined the Institute of Electronics Communications and Information Technology, Queen's University Belfast, in September 2009, as a Reader (an Associate Professor). In 2010, he was a Visiting Professor with UPCT, Spain. He has authored or coauthored over 150 peer-reviewed papers three book chapters and two patents. His research interests include modeling and design of microwave filters, frequency-selective surfaces and periodic structures, leaky wave antennas, and microwave sensing and curing as well numerical techniques for electromagnetics. He has held a research fellowship from Onassis Foundation, in 2001, a Research Fellowship from the U.K. Royal Academy of Engineering, between 2006 and 2011, and a European Marie-Curie Experienced Researcher Fellowship, in 2011. He was a co-recipient of the 2011 European Space Agency Young Engineer of the Year Prize, the 2011 EuCAP Best Student Paper Prize, and the 2012 EuCAP Best Antenna Theory Paper Prize.

DIMITRIS E. ANAGNOSTOU (Senior Member, IEEE) received the B.S.E.E. degree from the Democritus University of Thrace, Greece, in 2000, and the M.S.E.E. and Ph.D. degrees from the University of New Mexico, Albuquerque, NM, USA, in 2002 and 2005, respectively. From 2005 to 2006, he was a Postdoctoral Fellow with Georgia Tech, Atlanta, GA, USA. In 2007, he joined as an Assistant Professor with the South Dakota School of Mines and Technology, Rapid City, SD, USA, where he was promoted to an Associate Professor and received tenure. In 2016, he joined the Heriot-Watt University, Institute of Signals, Sensors, and Systems (ISSS), Heriot-Watt University, where he is currently a MSCA IF Fellow and an Associate Professor and Marie-Curie Fellow. He was with Kirtland AFB, NM, USA, and the Democritus University of Thrace. He has authored or coauthored more than 170 peer-reviewed papers (H-index: 30, Citations: >3450), holds two (2) USPTO patents and has one more UK/EU patent pending. His interests include reconfigurable electromagnetic devices (antennas, arrays, microwave circuits) using MEMS and novel material technologies (e.g. phase-change materials such as vanadium dioxide VO_2), radar, RF sensing, wearable electronics, artificial neural networks, security printing, and printable spacecraft - spanning applications from space satellites and defense to assisted living and consumer electronics (e.g. 5G/6G). He is a member of the Eta Kappa Nu (HKN) Honor Society, ASEE, and a Professional Engineer (PE) of the Technical Chamber of Greece (TEE). His research has been recognized worldwide and has received many prestigious awards. He has received the 2010 IEEE John D. Kraus Antenna Award, the 2011 DARPA Young Faculty Award by the U.S. Department of Defense, the 2014 ASEE Campus Star Award by the American Society for Engineering Education, the 2017 University of New Mexico Young Alumni Award, the SDSMT Honored Faculty Award (4 times between 2010 to 2014), and recently the prestigious H2020 Marie Skłodowska-Curie (MSCA) Individual Reintegration Fellowship (IF-RI) that supports his research during his transition to the EU. Many of his students have also been recognized with 15 IEEE and university awards such as the Heriot-Watt University Engineering Prize award, the SDSMT Best PhD Thesis award, IEEE AP-S Society travel grants, and others. He is a member of the IEEE-APS Educational Committee and the Co-Chair of Online Content, a member of the Technical Program Committee (TPC), and the Session Chair of IEEE-APS and EuCAP Intl' Symposia. He is also a Reviewer for international journals, such as *Nature* and IEEE Transactions. He serves or has served as an Associate Editor for the IEEE Transactions on Antennas and Propagation (two terms 2010 to 2016), the *IET Microwaves, Antennas and Propagation*, and IEEE Access, and as a Guest Editor for the IEEE Antennas and Wireless Propagation Letters (two special issues).